A Semigeostrophic Eady-Wave Frontal Model Incorporating Momentum Diffusion. Part III: Wave Dispersion and Dissipation

WILLIAM BLUMEN

Department of Astrophysical, Planetary, and Atmospheric Sciences, University of Colorado, Boulder, Colorado

(Manuscript received 1 May 1991, in final form 16 August 1991)

ABSTRACT

The two-dimensional, semigeostrophic and uniform potential vorticity Eady model is considered. An unstable baroclinic wave develops large velocity and temperature gradients in a narrow zone. Momentum diffusion and wave dispersion are incorporated into the model to prevent the ultimate development of a discontinuity in the alongfront geostrophic velocity v ($v_x = \infty$). Diffusion and dispersion act to reduce the amplitude of the growing baroclinic wave, and these processes also act to expand the width of the frontal zone, where the maximum velocity gradient is located. Explicit relationships are derived that reveal how these processes are dependent on two parameters: ϵ, the nondimensional eddy diffusion coefficient, and λ, the ratio of a dispersion coefficient μ to ϵ^2. The total dissipation of kinetic energy D is separated into two parts, D_1 and D_2: D_1 provides the dissipation that is largely confined to the relatively narrow frontal zone, and $D_2 = D - D_1$ provides the dissipation that is associated with the decaying waves that trail behind the front. These evaluations are carried out for a range of parameter values (ϵ, λ). Results show that the dissipation is not confined exclusively to the frontal zone but that $D_2 \leqslant D_1$ when λ is large. Limitations of the present model development are associated with the excessive growth of the unstable Eady wave in the absence of dissipation and the lack of fine-scale measurements that may be used to design a dynamical model of the frontal zone.

1. Introduction

Blumen (1990a,b; hereafter I and II) examined the evolution of an unstable semigeostrophic Eady wave for a period of time $t > t_c$. Here t_c is the critical time at which the alongfront geostrophic velocity v, associated with a semigeostrophic Eady wave, becomes discontinuous: the relative vorticity becomes infinite. This discontinuous behavior is removed, for $t > t_c$ by the introduction of momentum diffusion in a relatively thin layer where the horizontal gradient of v is a maximum, the frontal zone. Not only does momentum diffusion prevent the frontal collapse, an equilibration or even decay of the wave amplitude can occur, and the frontal zone expands with time. Both features are sensitive to the magnitude of the nondimensional eddy viscosity coefficient ϵ introduced into the frontal zone model. The solutions obtained from this model were also used to determine the dissipation of kinetic energy as a function of ϵ. The dissipation over a tropospheric layer extending from the ground to a midlevel, about 5 km, is about one to two orders of magnitude larger than dissipation rates that have been associated with the planetary boundary layer and with clear-air turbulence (1–5 W m^{-2}). Although frontal dissipation rates associated with this model are relatively large in a local region, the global contribution is about an order of magnitude less than that associated with boundary-layer dissipation. It does appear, however, that frontal zone dissipation may make a significant contribution to dynamical processes associated with the life cycle of a midlatitude cyclone.

It is not certain whether the model provides reasonable dissipation rates, since measured values from surface-based fronts are not presently available. Kennedy and Shapiro (1980) did, however, use aircraft measurements and inertial subrange theory to provide the dissipation rate in an upper-level front. Their value of the dissipation rate in a frontal zone extending over a depth of 5 km is estimated to be about 75 W m^{-2}, or one to two orders of magnitude larger than values that have been associated with both the planetary boundary layer and clear-air turbulence. Values of the dissipation rate in the frontal model, presented in I and II, may either be smaller or larger than the value associated with the upper-level front, depending on whether the model front has equilibrated or not. This basis for comparison provides some support for use of the theoretical model to examine physical processes associated with frontal-zone dynamics not considered in I and II.

In particular, the previous model examines a frontal zone of finite width maintained solely by momentum diffusion within the zone. The present development relaxes this limitation by the introduction of wave dispersion, which may act in concert with momentum

Corresponding author address: Dr. William Blumen, Department of Astrophysical, Planetary, and Atmospheric Sciences, University of Colorado, Campus Box 391, Boulder, CO 80309-0391.

diffusion to limit the unstable amplitude growth, to affect the characteristic frontal zone width, and to provide dissipation in the wave train that trails behind the front.

There is ample observational evidence to document the existence of mesoscale wave disturbances in the atmosphere. For example, Uccellini and Koch (1987) summarize 13 case studies of wave disturbances with periods of 1–4 h and horizontal wavelengths of 50–500 km. These authors note that there have been attempts to show that the observed wave motions are internal gravity waves or, perhaps, gravity–inertia waves when the effect of the earth's rotation is nonnegligible. The source of these wave motions has not been definitively established. There are undoubtedly various sources that involve some type of atmospheric imbalance, for example, convection, turbulence, and shear instability. Uccellini and Koch note that momentum (or heat) imbalances lead to excitation of gravity–inertia waves as a natural consequence of the geostrophic adjustment process, although other mechanisms are not excluded. It is noteworthy, however, that a "distinct frontal boundary" is a feature that is common to all cases. Further, the waves tend to be associated with a lower-tropospheric temperature inversion and appear in the cold air behind a stationary front or ahead of a warm front.

The presence of a frontal zone, where momentum, or heat imbalances, or both are likely, constitutes the basic core of the present investigation. The wave source is postulated to be associated with a frontal zone of finite extent, say $L \sim 100$ km, above the boundary layer, which is comparable with observed values (Keyser and Shapiro 1986). Within the frontal-zone convective and turbulent mixing, shear instabilities and possibly other dynamical imbalances provide the mechanisms that lead to both momentum diffusion and wave dispersion that limit further frontal collapse. It is not possible, without fine-scale measurements, to isolate particular mechanisms (e.g., Uccellini and Koch 1987). No attempt will be made here to propose a specific source for these waves. Rather, two models presented by R. R. Long will be used to demonstrate that solitary waves may be initiated in either a density stratified environment or in a well-mixed region (a homogenous fluid). In the former case, the solitary wave may be characterized as an internal gravity wave; in the latter case as an inertial wave. Long's model developments lead to the Korteweg–deVries (KdV) equation. The present extension, which takes account of momentum diffusion, leads to the KdV–Burgers equation. These models are not necessarily models of actual frontal zone dynamics but are presented to indicate the generic nature of the KdV–Burgers equation in a geophysical context.[1]

[1] In some cases the Benjamin–Davis–Ono (BDO)–Burgers equation may be more appropriate (e.g., Christie 1989).

The present focus is not on the derivation of the KdV–Burgers equation (2) but on the principal effects of momentum diffusion and wave dispersion on frontal characteristics. Consequently, the development of (2) will be relegated to appendix A, and most of the details may be found in Long (1953, 1965, 1971). The reader may, however, skip appendix A since the basic results are reproduced in section 2.

A model is presented in section 2 that takes account of diffusion and dispersion in association with a frontal zone. Solutions are presented as a function of the parameter λ, which provides a measure of the relative importance of dispersion versus diffusion. Frontal characteristics, including the frontal zone width and vertical cross sections of the front, are displayed in section 3. The solution developed in section 2 is used to interpret some of the frontal properties displayed in Fig. 3. This presentation appears in section 4. Finally, calculations of the depth-averaged dissipation rate, presented in section 5, are separated into two parts: one without the superposed wave motion, designated as D_1, and one representing the total dissipation that includes the waves, designated as D. The contribution to the dissipation that results from the presence of the waves is $D_2 = D - D_1$. The relative amount of dissipation that may be associated with D_2 can be as large as 50% of the total amount. The implications are discussed in the final remarks of section 6.

2. Model and solutions

The rationale for the present model development is provided in I (see section 2). The two-dimensional, uniform potential vorticity Eady model is employed. Unstable, inviscid solutions of this model are used for $t > t_c$. The alongfront geostrophic velocity is $v(x, z, t)$, where x is normal to the front and directed to the east, z is the vertical coordinate, and t is time. Momentum diffusion embedded in a thin layer prevents the occurrence of an infinity in relative vorticity or a multivalued solution. It is assumed in I that, within the frontal zone, a balance between nonlinear advection and momentum diffusion is achieved. Nonlinear advection steepens the wave, leading to $\partial v/\partial x = \infty$ at $t = t_c$. Diffusion prevents this type of breakdown, and a frontal zone of finite width characterizes the model solution.

Here it is proposed that the frontal zone achieves a balance between nonlinear advection, momentum diffusion, and wave dispersion. As in I, a variable V is defined to be

$$V = \frac{v}{Ae^{\sigma t}}, \tag{1}$$

where $A(k, z)$ is the amplitude and σ is the growth rate of the unstable Eady wave characterized by wavenumber k. The frontal balance is expressed by

$$-V\frac{\partial V}{\partial x} - \epsilon\frac{\partial^2 V}{\partial x^2} + \mu\frac{\partial^3 V}{\partial x^3} = 0, \tag{2}$$

where ϵ is a nondimensional eddy viscosity coefficient and μ is a nondimensional measure of the wave dispersion; the characteristic scales for all variables, typical of midlatitude synoptic scale flow, are provided in I (section 2). Equation (2) is the KdV–Burgers equation (e.g., Grad and Hu 1967; Johnson 1970; Karpman 1975). The two limiting cases are $\mu = 0$, the Burgers equation, and $\epsilon = 0$, the KdV equation. The former case has been examined in the context of the present model in I. The latter case provides a solitary wave solution presented, for example, by Long (1965). A rationale for the proposed balance represented by (2) is presented in appendix A.

a. Approximate solution

There are apparently no known analytical solutions of (2) when $\epsilon \neq 0$ and $\mu \neq 0$; therefore, a numerical evaluation will be made. First, however, an approximate solution that exhibits the physical properties of momentum diffusion and wave dispersion most simply will be presented.
A new variable,

$$y = \frac{x}{\epsilon}, \tag{3}$$

is introduced into (2) to yield

$$-V\frac{\partial V}{\partial y} - \frac{\partial^2 V}{\partial y^2} + \lambda\frac{\partial^3 V}{\partial y^3} = 0, \tag{4}$$

where $\lambda = \mu\epsilon^{-2}$. This parameter λ provides a nondimensional measure of the relative magnitude of wave dispersion to momentum diffusion. A physical interpretation of this parameter λ may be extracted from (A10), which may be treated as an order of magnitude estimate for present purposes. The parameter ϵ provides a measure of the relative importance of momentum diffusion; the parameter $\mu \sim \gamma\beta^{-2}$ is associated with wave dispersion, where $(\beta, \gamma, \epsilon)$ are defined below (A7). In the *stretched coordinate representation* the parameter λ is approximately

$$\lambda \sim \frac{\gamma}{\beta^2\epsilon^2} = (\nu b U^{-1})^{-2}, \tag{5}$$

where ν is the eddy viscosity coefficient, $b = -(\ln\bar{\rho})_{\bar{z}}$, and U is a characteristic zonal velocity within the frontal zone. Consequently, $\lambda^{1/2}$ may be interpreted as a Reynolds number, where b^{-1} is the characteristic scale of the relatively weak vertical density gradient within the frontal zone.

The case of a well-mixed (homogeneous) frontal zone with an Ekman suction velocity w_0 at the lower boundary is also considered in appendix A. In this example, b^{-1} is the characteristic scale of the horizontal variation of w_0 across the frontal zone, and U is replaced by w_0 in (5).

One integration of (4) provides

$$-\frac{1}{2}V^2 - \frac{\partial V}{\partial y} + \lambda\frac{\partial^2 V}{\partial y^2} = \frac{1}{2}B, \tag{6}$$

where B is a function of time. A composite solution will be derived in which the frontal zone solutions of (6) will be matched to an inviscid solution that satisfies

$$\left(\frac{\partial}{\partial\tau} - V\frac{\partial}{\partial x}\right)V = 0, \quad -\pi \leqslant x \leqslant \pi. \tag{7}$$

The transformed time variable is defined as

$$\tau = kA\,\mathrm{Ro}e^{\sigma t}, \tag{8}$$

where (k, σ, A) are defined below (1), and $\mathrm{Ro} \leqslant 0.3$ denotes the Rossby number. The manner in which the matching is carried out for $\lambda = 0$ is discussed in section 2 and developed in the Appendix of I. The rationale and mathematical development is unchanged when $\lambda \neq 0$; The reader may refer to this cited material for details that are omitted here.

As $|y| \to \infty$, the solution of (6) reduces to

$$\left.\begin{aligned} V &\to -H(\tau), \quad y \to -\infty \\ V &\to \ \ H(\tau), \quad y \to \infty \end{aligned}\right\}, \tag{9}$$

where $H(\tau) = \beta\tau^{-1}$ and β is a solution of $\beta^{-1}\sin\beta = \tau^{-1}$. Then the arbitrary function of time $B(\tau)$ in (6) is $B = -H^2$, and we seek solutions of

$$\lambda\frac{\partial^2 V}{\partial y^2} - \frac{\partial V}{\partial y} - \frac{1}{2}V^2 = -\frac{1}{2}H^2. \tag{10}$$

The solution of (10) for $\lambda = 0$ that is matched to the solution of (7) is presented in I by (10a, b).

An approximate solution of (10) that illustrates the dispersive characteristics of the waves will be provided before the composite solution is examined. It is shown in appendix B that the waves are present behind the front, $y < 0$. This representation is completely arbitrary in the present context. The choice is based on some observational results presented by Uccellini and Koch (1987). The waves will appear ahead of the front if the sign before the viscous term is changed in (2). Following Karpman (1975), a solution in this region may be expressed as

$$V = -H + f(y, \tau). \tag{11}$$

For present purposes it is assumed that $f \ll H$. Introduction of (11) into (10) yields the linear equation:

$$\lambda f'' - f' + fH = 0, \tag{12}$$

where the prime notation denotes $\partial/\partial y$. The solution of (10), taking note of (11) and (12), is

$$V = -H + C\exp\left(\frac{y}{2\lambda}\right)\sin\left[\left(H\lambda - \frac{1}{4}\right)^{1/2}\frac{y}{\lambda}\right], \quad y < 0, \tag{13}$$

where $C = C(\tau, \lambda)$, λ is defined by (5), and $H\lambda > \frac{1}{4}$. Since $y = x/\epsilon$, the waves are damped with distance

behind the front at a rate $(2\epsilon\lambda)^{-1}$. The wavelength is given by

$$\frac{L}{\epsilon} = 2\pi\lambda\left(H\lambda - \frac{1}{4}\right)^{-1/2}. \tag{14}$$

The wavelength L changes with time $\tau(t)$ as $L \propto H^{-1/2}$. Since H, defined below (9), is a decreasing function of τ, the wavelength of the trailing waves increases with time. Some characteristic values of L, shown in Fig. 1, illustrate the significant dependence on the relevant parameters $(\epsilon, \lambda, \tau)$.

b. Numerical solution

Numerical solutions of (10), for constant H, have already been presented by Grad and Hu (1967) and Johnson (1970), among others. The succinct phase-plane analysis, presented in appendix A, follows that of Grad and Hu. It is demonstrated that waves occur behind the front only if $\lambda H > \frac{1}{4}$; otherwise, V increases monotonically with x, as in the case $\lambda = 0$. Present purposes are also served by making use of the analysis to provide starting values of V and $\partial V/\partial y$ in the numerical evaluation of (10).

A numerical solution of (10) is displayed in Fig. 2 for different values of λ. The dashed curves represent the approximate solution (13), where $C(\tau, \lambda)$ has been adjusted to provide the best fit. It is apparent that the linearization has retained the principal features associated with the damping rate and the characteristic wavelength.

3. Frontal characteristics

A composite solution of the alongfront velocity V is obtained by matching the inviscid solution of (7) to the frontal zone solution of (10). The region of overlap, where both solutions are valid, is provided by $|x| \to 0$ for the inviscid solution and $|y| \to \infty$ for the frontal zone solution. Both limits are independent of λ. Consequently, the mathematical formalism is that provided in the Appendix of I, which is also appropriate for $\lambda \neq 0$. Similarly, the scaled potential temperature Θ, defined in the Appendix of I below (A13), may also be evaluated by the same approach. There is, however, a minor error in the determination of Θ that is corrected in appendix C. This error has no effect on any of the results or conclusions presented in I.

Solutions for the cross-front velocity v, and the potential temperature perturbation θ are displayed in Figs. 3 and 4. The parameter values chosen for display are $\epsilon = 5 \times 10^{-2}$ and $\lambda H(\tau = 2.37) = 4$ and 16. Values of $H(\tau)$ are exhibited in Table 1. The values of λ, corresponding to $\lambda H = 4$ and 16, are $\lambda = 4.569$ and $\lambda = 18.275$. Comparison with the case $\lambda = 0$, presented in Figs. 2 and 3 in I, provides a clear indication of the dependence of the wave characteristics on the parameter λ that is defined in (5).

The wave characteristics that are evident in these figures have been examined in the model solution developed in section 2. At any level z, the wavelength increases with time as exhibited by (14). Further, the wavelength *decreases* with height z. This latter circumstance is associated with the fact that τ, defined

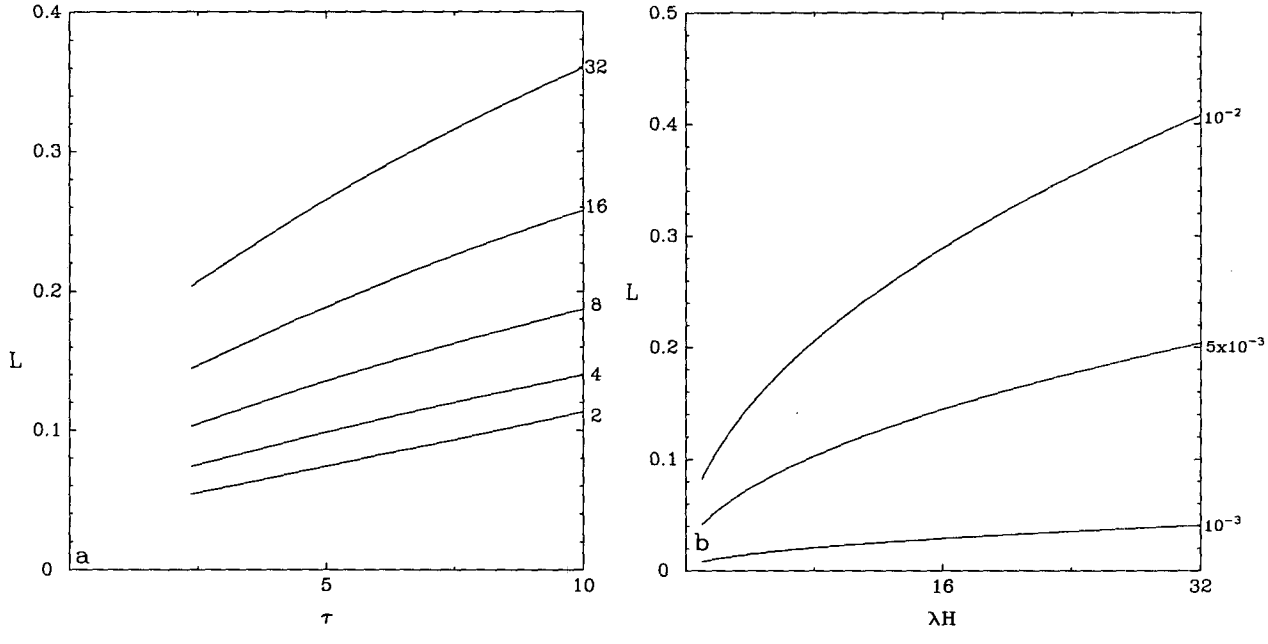

FIG. 1. (a) Wavelength L, given by (14), as a function of the time variable $\tau(t)$ defined by (8). The labels along the right ordinate represent λH at $\tau = 2.37$, the starting values, and the curves are associated with a diffusion parameter $\epsilon = 5 \times 10^{-3}$. $L = 10^{-1}$ corresponds to 62×10^3 m, and the time in days is presented in Table 1. (b) As in (a) except L as a function of λH for the three values of ϵ appearing along the right ordinate.

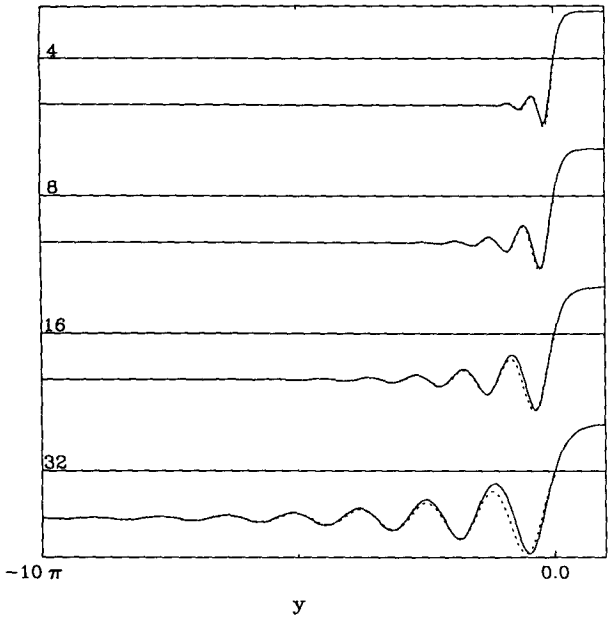

FIG. 2. The solution of (10) for V, defined by (1), as a function of the stretched variable $y = \epsilon^{-1}x$. The labels along the left ordinate represent λH at $\tau = 2.37$, and $V = V(y, 2.37)$. The dashed curves represent the approximate solution given by (13).

by (8), decreases with z since A is a decreasing function of z. However, H, defined below (9), is an increasing function of z, as shown in Table 1. It is also noteworthy that the wave train tends to exhibit fewer waves as τ increases. This circumstance is associated with the fact that λ is held constant in these evaluations so that λH decreases with time. The solution of (10) becomes a monotonically increasing function of x as $\lambda H \to \frac{1}{4}$, as shown in appendix B. The dependence of the solution on the diffusion parameter ϵ is contained in the stretched variable y, defined by (3). Both the exponential damping rate of the waves and their wavelength are affected by the value of ϵ, as shown by (13) and (14). In particular, the wavelength L is a linearly increasing function of ϵ, for λ constant. Consequently, the characteristics of (v, θ) in Figs. 3 and 4, for values of ϵ either larger or smaller than $\epsilon = 5 \times 10^{-2}$ are determined by the transformation between x and the stretched variable y.

The manner in which both parameters ϵ and λ affect the wave amplitude is displayed in Fig. 5. The ordinate of this figure is the magnitude of the minimum value of v, the trough of the first wave, as shown for example in Figs. 3 and 4. It is evident here, as in the case $\lambda = 0$ (Fig. 8 of I), that momentum diffusion is one means of offsetting the exponential amplitude growth associated with baroclinic instability. Examination of Fig. 5 shows that wave dispersion ($\lambda \neq 0$) may also counteract exponential growth, and the effect may be significant. (Compare Fig. 5 with Fig. 8 in I). The damping of the amplitude is not a monotonic function of λ or λH: the maximum effect is associated with λH ($\tau = 2.37$) = 4. An analysis will be presented in the following section.

Another feature that is affected by the presence of waves is the thickness of the frontal transition zone. For present purposes, this zone is defined to be the distance between the minimum and maximum values of v: the waves are assumed to trail behind the frontal zone. This distance Δx is shown as a function of τ in Fig. 6 for various values of ϵ and λ. The comparable evaluation for $\lambda = 0$ is shown in Fig. 6 of I. As in I, the frontal zone expands with a relative increase in the magnitude of momentum diffusion ϵ. The frontal zone expansion is also a monotonically increasing function of λ, at least for the parameter range considered. These characteristics, in which diffusion and wave dispersion work in concert to prevent the occurrence of an infinite relative vorticity ($\partial v/\partial x \to \infty$), represent the cornerstone of the present model.

4. Analysis of frontal characteristics

The linear solution of (10), given by (13), provides a valuable means to interpret the wavelike characteristics that are displayed in Figs. 3 and 4. This solution is also used to analyze the frontal-zone characteristics that are displayed in Figs. 5 and 6.

The function $C = C(\tau, \lambda)$, defined by (13), is determined by a numerical curve fitting procedure. For present purposes, the relatively weak dependence of C on λ may be neglected, and C may be represented as

$$C = H(\tau). \tag{15}$$

Now, it is a straightforward evaluation to determine both the *position and the magnitude* of the minimum value of

$$v = Ae^{\sigma t}V \propto \tau V. \tag{16}$$

This evaluation shows that a very good approximation is

$$v \propto \tau H(\tau) \exp\left[-\frac{\pi}{4}\left(H\lambda - \frac{1}{4}\right)^{-1/2}\right], \quad \lambda \gtrsim 4. \tag{17}$$

In essence, this approximation may be derived by setting

$$\frac{(H\lambda - 1/4)^{1/2}y}{\lambda} = -\frac{\pi}{2} \tag{18}$$

in (13) to get the minimum value of V and then evaluating the exponential with (18).

The amplitude v, expressed by (17), is an increasing function of λ when τ is held constant. Numerical evaluations, displayed in Fig. 5 and Fig. 8 of I, show that as $\lambda \to 0$ the amplitude of v also increases. In the absence of both momentum diffusion and wave dispersion, the wave amplitude will grow without bound according to $v \propto \tau \propto \exp\sigma t$. The present results show that there is an optimal $\lambda = \mu\epsilon^{-2}$, with ϵ constant, that

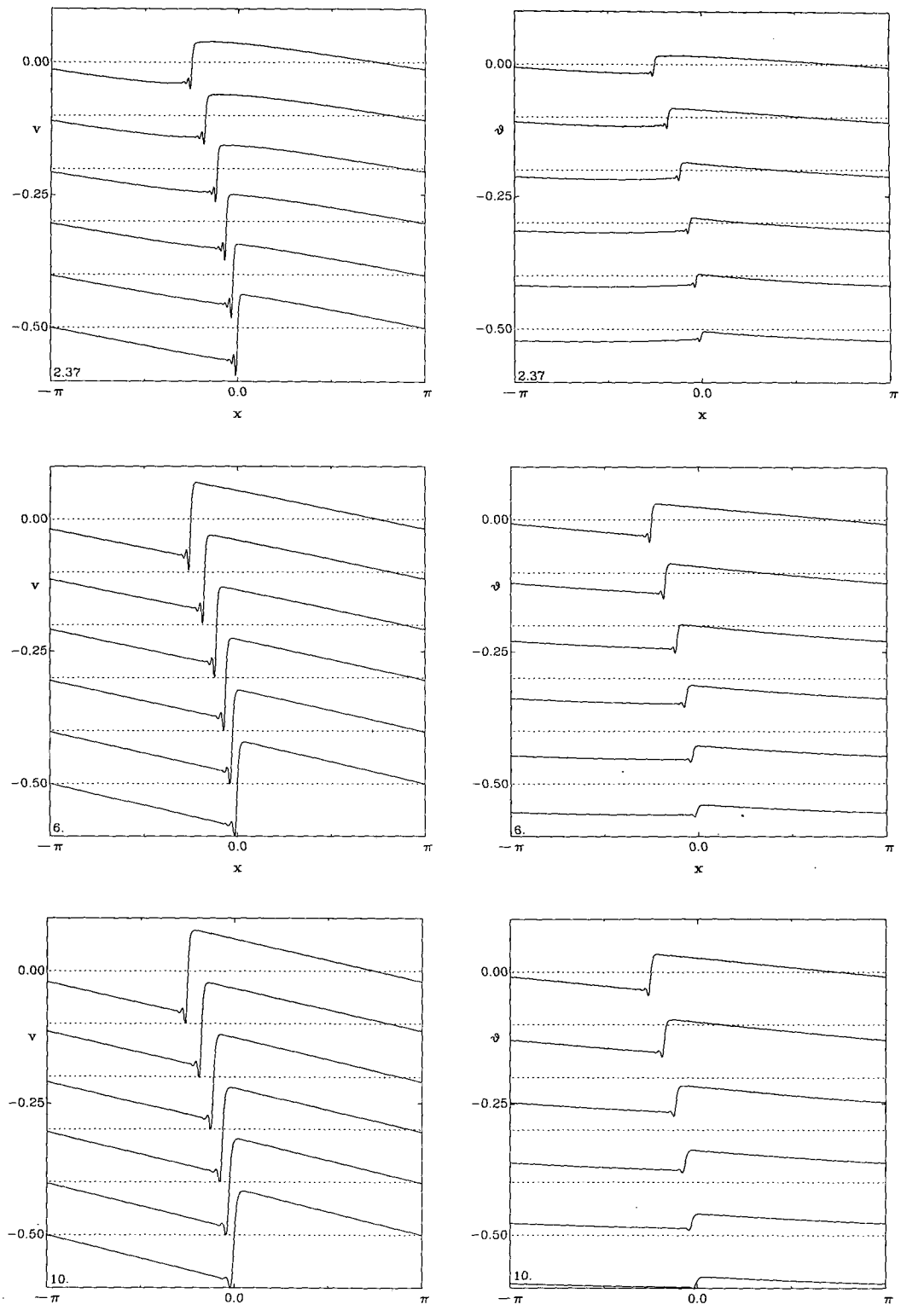

FIG. 3. Alongfront velocity v (left) and potential temperature perturbation θ (right) as functions of the horizontal coordinate x. These solutions, associated with $\lambda H = 4$ at $\tau = 2.37$, are displayed at different vertical levels between the lower boundary $z = -0.5$ and the midlevel $z = 0$. Values of the time τ appear in the lower left-hand corner.

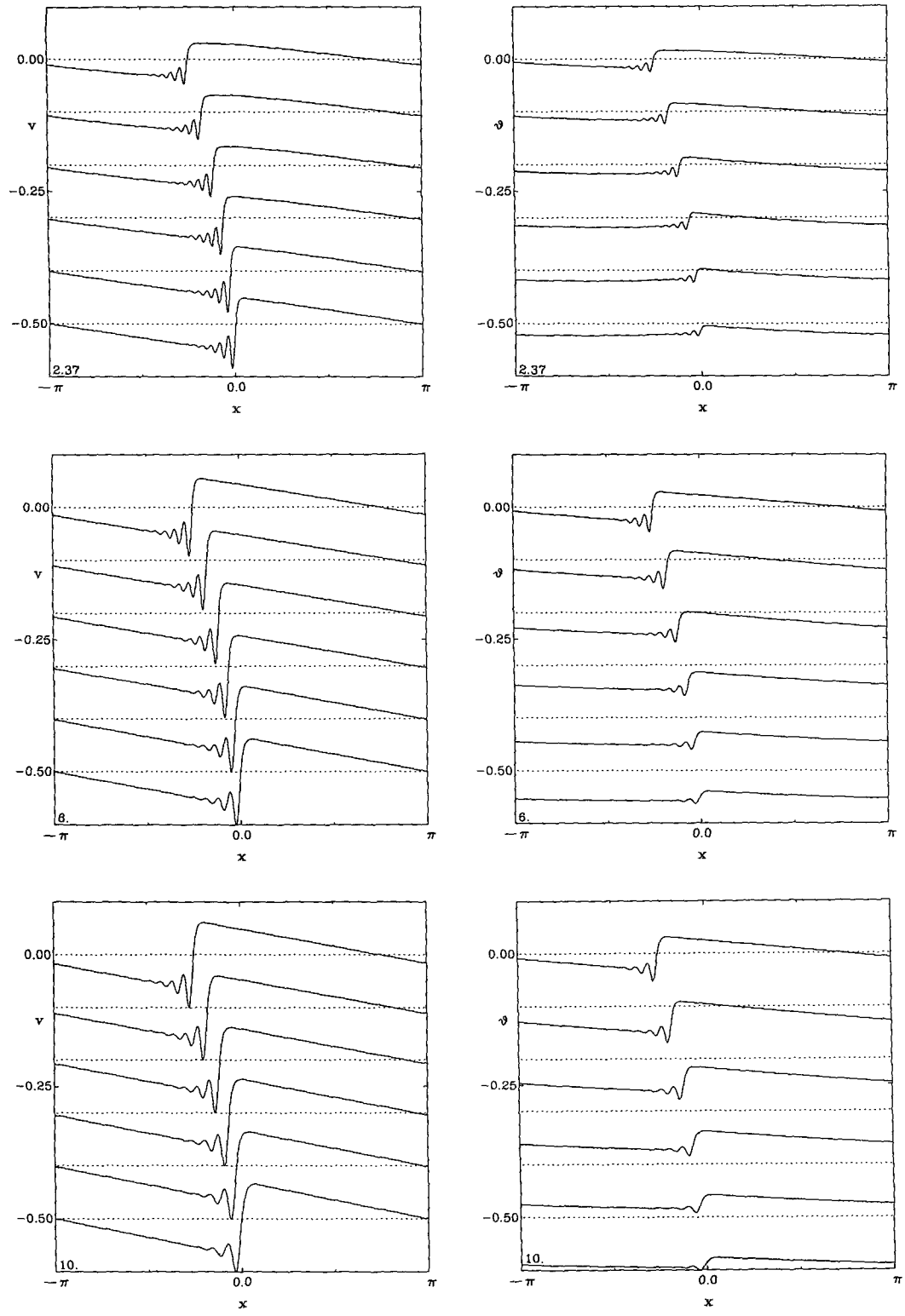

FIG. 4. As in Fig. 3 except that $\lambda H = 16$ at $\tau = 2.37$.

will counteract this unstable growth. The function H is a decreasing function of τ (Table 1), and exponential damping associated with $\lambda \neq 0$ increases with decreasing values of λ ($\lambda \gtrsim 4$). The characteristic properties of (17), displayed in Fig. 7, are in accord with panels (b) and (c) in Fig. 5.

TABLE 1. Values of $H(\tau)$ at the ground ($z = -0.5$) and at midlevel ($z = 0$) as a function τ. The corresponding value of t, determined for Ro = 0.3, is expressed in days.

t(d)	$\tau(-0.5)$	$H(-0.5)$	$\tau(0)$	$H(0)$
4.33	2.37	0.8755	1.25	0.9053
5.49	6.00	0.4465	3.17	0.7326
6.12	10.00	0.2852	5.28	0.4969

The expansion of the frontal zone exhibited in Fig. 6 is not entirely associated with the solution for $y < 0$, since the position of the maximum value of v is not considered. Yet the expression

$$|y| = \frac{\pi}{2}\lambda\left(H\lambda - \frac{1}{4}\right)^{-1/2} \tag{19}$$

shows the monotonic growth of the frontal zone, as the position of the first wave trough is displaced to the left (decreasing x). The estimate provided by (19) $|y| \propto \lambda^{1/2}$ for fixed τ is an overestimate of the increase of the frontal zone with λ that is provided in Fig. 6, but is not out of line. The increase of the frontal zone that arises from the variation of ϵ, encompassed in the stretched variable y, has been considered in section 3.

5. Kinetic energy dissipation

A principal feature of this model is the presence of physical processes that can equilibrate the unstable wave or, depending on the parameter values, can damp the wave. Computations of the kinetic energy dissipation in II, associated with momentum diffusion alone ($\lambda = 0$), showed that relatively large dissipations are associated with the relatively large development of frontal gradients in the unstable wave. The values determined are at least an order of magnitude larger than the maximum values of $\epsilon \approx 5$ W m^{-2} associated with both clear-air turbulence and boundary-layer dissipations. The total dissipation that characterizes the present model is unaltered by the presence of waves ($\lambda \neq 0$). All of the dissipation is associated with momentum diffusion. When $\lambda \neq 0$, however, not all of the dissipation occurs in the frontal zone; a portion occurs in the region occupied by the wave train.

The total dissipation, defined as in I [e.g., Eq. (18)], is

$$D = \epsilon\tau^3 \int_{-0.5}^{0} \frac{1}{2\pi} \int_{-\pi}^{\pi} \left(\frac{\partial V}{\partial x}\right)^2 dxdz, \tag{20}$$

where $V = v\tau^{-1}$ and the integration is carried out over one wavelength and from the ground to midlevel ($\approx$5 km). All of the dissipation calculations in II were carried out as prescribed by (20). Some corrections to expressions appearing in II are made in the present appendix C.

An asymptotic evaluation was carried out in II, where it is shown that $D \approx$ const for $(2\epsilon)^{-1} \gg \tau \gg 1$

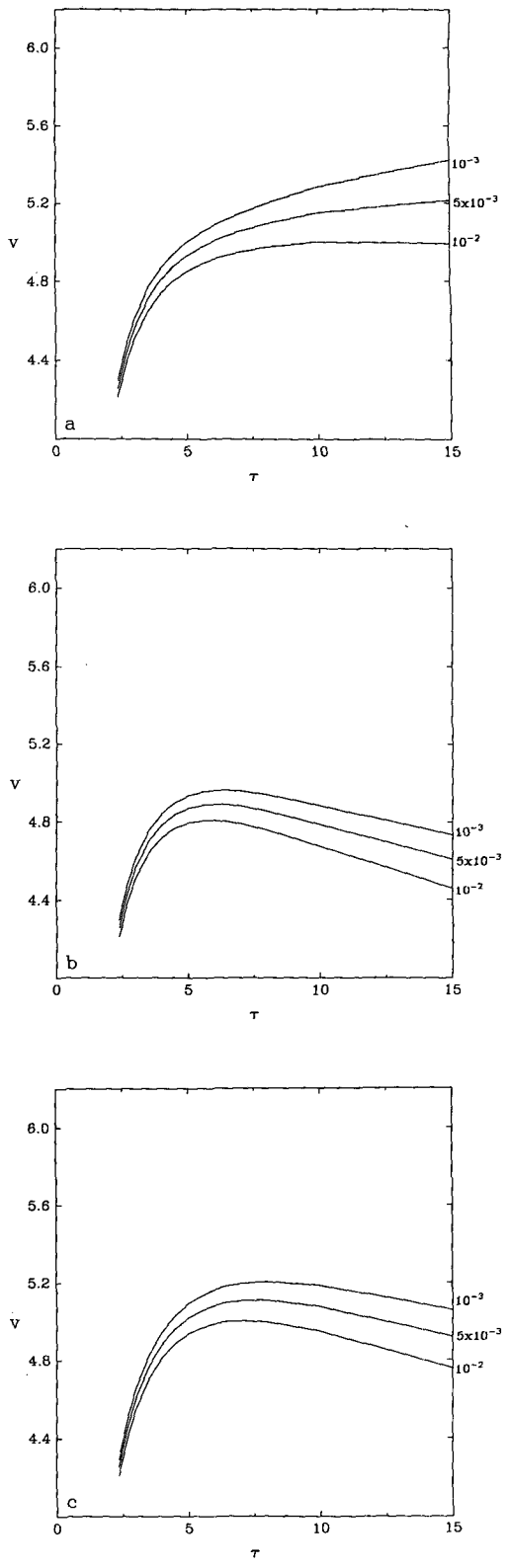

FIG. 5. The magnitude of the alongfront velocity v at the left edge of the frontal zone $x < 0$ as a function of time τ: v is represented in units of the zonal velocity. The curves are associated with the three values of ϵ appearing along the right ordinate. (a) $\lambda H = 1$ at $\tau = 2.37$. (b) $\lambda H = 4$ at $\tau = 2.37$. (c) $\lambda H = 16$ at $\tau = 2.37$.

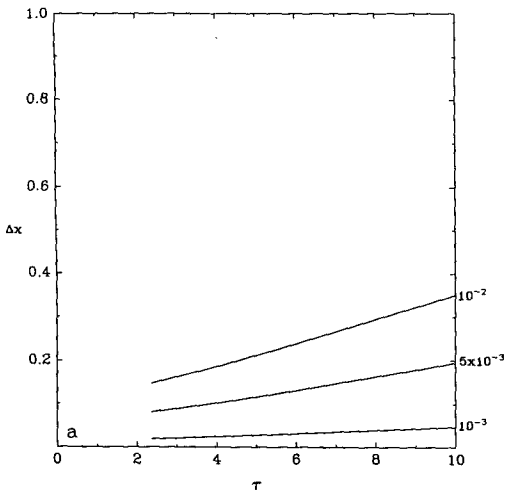

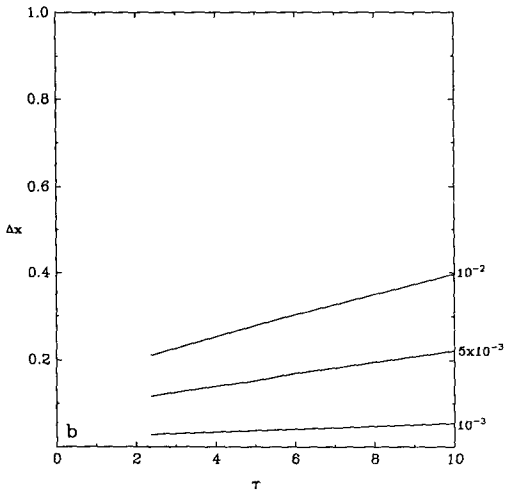

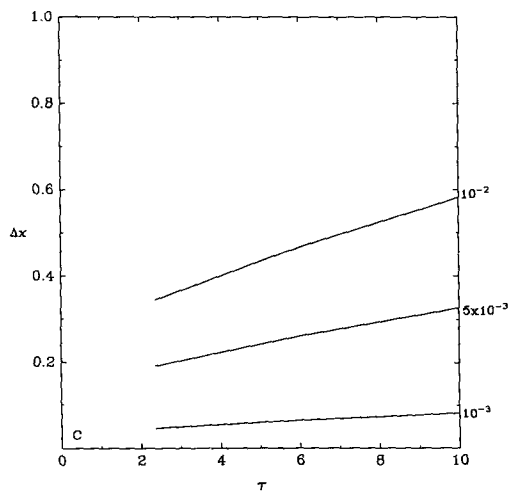

FIG. 6. As in Fig. 5 except Δx, the width of the frontal zone, as a function of τ. $\Delta x = 0.10$ corresponds to 62.2×10^3 m.

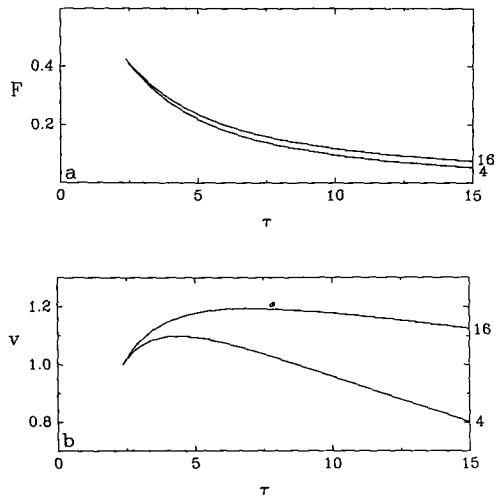

FIG. 7. (a) Evaluation of $F = v\tau^{-1}$, defined in (17), as a function of τ. The curves correspond to $\lambda H = 4$ and 16 at the initial time $\tau = 2.37$. (b) The normalized velocity $v = \tau F$, defined in (17), as a function of τ.

and $\epsilon \leqslant 10^{-2}$. Essentially, all of the dissipation occurs in the frontal zone, whose scale in the stretched variable $y = x/\epsilon$ is independent of ϵ.

In the present model, significant dissipation is associated with the decaying wave train outside the frontal zone. The computations were carried out as follows. The total dissipation is determined from the full solution, including the waves, as shown in Figs. 3 and 4. Next, the waves to the left of the minimum value of v were removed, and the dissipation again computed from (20). This value, denoted by D_1, is the counterpart of the evaluation in II, since the waves are not present. Yet this computation is indirectly affected by waves, since the minimum value of v and the frontal width are functions of λ. Finally, the part of the dissipation that is presumed to occur in the wave train is determined as the residual $D_2 = D - D_1$.

The results are displayed in Fig. 8. The values chosen for display correspond to $\lambda H = 8$ and 32 at $\tau = 2.37$ ($\lambda = 9.138$ and $\lambda = 36.551$). The larger value was chosen because, initially, the dissipation associated with the frontal zone and the dissipation in the wave train are equal. As time evolves, increasing τ, λH begins to decrease (see Table 1), and momentum diffusion becomes relatively more important than wave dispersion. This is evident in the bifurcation of the $D_1(32)$ and $D_2(32)$ curves. The same feature appears in the $D_1(8)$ and $D_2(8)$ curves, but for this parameter value $\lambda H = 8$ ($\tau = 2.37$), almost three times as much dissipation occurs in the frontal zone at the initial time.

These evaluations have been made for $\epsilon = 5 \times 10^{-3}$, and the values of D are essentially insensitive to variations of $\epsilon \leqslant 10^{-2}$. However, the extent of the region where the waves dissipate kinetic energy will be extended or compressed according to whether ϵ is larger or smaller than $\epsilon = 5 \times 10^{-3}$.

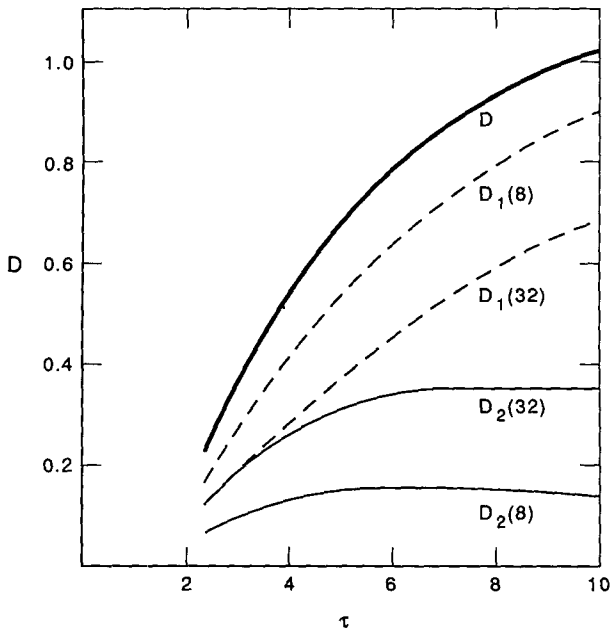

FIG. 8. Dissipation D, defined by (20), as a function of time τ. The definitions of D_1 and D_2, associated with $\lambda H = 8$ and $\lambda H = 32$ at $\tau = 2.37$, are provided in the text. The dissipation is associated with $\epsilon = 5 \times 10^{-3}$. $D = 1$ corresponds to 240 W m^{-2}.

6. Final remarks

Properties of a semigeostrophic Eady model that incorporates wave dispersion and momentum diffusion have been examined. The aim has been to expose the relative importance of these two physical processes in a relatively simple model that can simulate frontogenesis. Dispersion and diffusion counteract unstable baroclinic growth.

The present results establish that there is an optimal ratio of wave dispersion to momentum diffusion, $\lambda \approx 4$, that will provide the maximum retardation of amplitude growth and will ultimately lead to amplitude decay. Equation (5) shows that this optional value implies that the scale of the vertical density variation b^{-1}, within the frontal zone, is about twice as large as the characteristic viscous scale νU^{-1}. This feature is displayed in Fig. 5.

The model results show that the frontal zone of width Δx will expand with an increase of either ϵ or λ: momentum diffusion and wave dispersion both promote frontolysis. A relatively simple expression for Δx can be derived when $\lambda \gtrsim 4$, providing the approximate representation $\Delta x \sim \epsilon\lambda^{1/2}$; that is, the frontal zone expands in direct proportion to b^{-1}.

Finally, the relative importance of wave dispersion, in distributing the kinetic energy dissipation between the region of the frontal zone itself and the region of the decaying wave train behind the front, has been demonstrated by the calculations displayed in Fig. 8. This latter result could be of importance in the development of mesoscale models that must resort to the parameterization of subgrid-scale processes that are responsible for dissipation in the model. It may be important to place the dissipation in the appropriate location, particularly if this dissipation is much larger than that associated with boundary-layer processes. This problem cannot be resolved by the present study: both observations and numerical experimentation are required.

Principal limitations associated with the present development appear to be 1) the unbounded growth of the baroclinic wave associated with the inviscid dynamics of the semigeostrophic Eady model, and 2) uncertainty in the representation of frontal zone dynamics encompassed in (4) or (10). Some simple representations have, however, been explored in appendix A.

It was noted earlier in I that Nakamura and Held (1989) found, from their primitive equation numerical model experiments, that equilibration of an unstable Eady wave could be attained by a change in the vertical structure of the wave. This latter process does not appear to be critically dependent on the type of model diffusion. It was suggested in I that ageostrophic accelerations, omitted from the semigeostrophic model, might promote the equilibration process found by Nakamura and Held. An alternative explanation is associated with the present method of solution rather than with the distinction between semigeostrophic and primitive equation dynamics. As in I, the inviscid dynamics of the present model, expressed by (7), is required to apply at all times. Wave steepening, effected by the nonlinear advection term in (7), is counteracted by diffusion and dispersion inherent in (4). In essence, the inviscid solution influences the frontal zone response, through the introduction of $H(\tau)$ in (9) and its presence in (10), but the frontal zone exerts no back effect on the inviscid dynamics. This influence of the frontal zone on the exterior region is presumably the reason that the solutions diverge from each other after about one week in real time. The Nakamura and Held solution is undoubtedly a more valid response at large times, which are not considered in the present study (see Table 1). Nonetheless, excessive alongfront velocities ($v \sim 100$ m s^{-1}) appear in both models; therefore, there is a basic model deficiency that needs to be remedied.

The second limitation, noted above, is the treatment of dynamics associated with the frontal zone. The present results can only provide an indication of the relevant importance of dispersion and diffusion associated with frontal zone circulations by means of some model assumptions (see appendix A). The nature of these circulations, the source of wave motions that propagate from the zone, and perhaps, preferred locations of turbulent dissipation are largely undocumented. The improvement of observational capabilities on the frontal scale will undoubtedly be closely followed by more refined modeling efforts.

Acknowledgments. Financial support for this investigation has been provided by the National Science

Foundation under Grants ATM-8820164 and ATM-9100171. Discussions with Richard Rotunno concerning the discrepancy between the Nakamura and Held results and the present model results are gratefully acknowledged. Thanks are also extended to Fei Wu for programming assistance.

APPENDIX A

A Derivation of the Korteweg-de Vries–Burgers Equation

Long (1965, 1971) presented two models, each of which contained solitary wave solutions governed by the KdV equation. The 1965 development is based on his earlier model work (Long 1953), which is usually referred to as Long's model. Two-dimensional, steady, nonlinear disturbances with an arbitrary vertical distribution of density and velocity are considered.[2] The present application follows Long (1965) in consideration of a uniform flow U and a relatively weak density gradient. The fundamental equation of Long's model may be expressed as

$$\nabla^2\psi + \frac{1}{\rho}\frac{d\rho}{d\psi}\left[\frac{1}{2}(\nabla\psi)^2 + gz\right] = H(\psi), \quad \text{(A1)}$$

where $\nabla^2\psi$ is the relative vorticity about a horizontal axis normal to the vertical (x, z) plane, ψ is the stream function, $u = \psi_z$ and $w = \psi_x$ are the (x, z) velocity components, $\rho = \rho(\psi)$ is the density, g is the acceleration of gravity, and $H(\psi)$ is determined by upstream conditions. In the present case the density gradient is

$$\frac{1}{\bar\rho}\frac{d\bar\rho}{d\psi} = -\frac{1}{\bar u}\frac{1}{\bar\rho}\frac{d\bar\rho}{d\bar z} = \frac{b}{\bar u}, \quad \text{(A2)}$$

where $\bar u = -\psi_{\bar z}$, $\bar z$ is the undisturbed height of the streamline $\psi = \text{const}$ and b provides the measure of the density gradient. This model is used by Long to show that the internal solitary wave represents a solution of (A1) under the condition $bh = \beta \ll 1$, where h is the fluid depth. The details need not be displayed; every step in the development is clearly exposed by Long.

It is proposed that Long's model represents the flow within a frontal zone, where the static stability may be expected to be relatively small due to mixing processes. The zone is a source of internal gravity-wave activity, and earth's rotation is not taken into account. The edges of the cross section at $|x| = \infty$, in a suitably scaled coordinate, represent the limits of the frontal zone. The frontal slope of order 10^{-2} is neglected to provide a simpler analysis, although this feature may be included by simple coordinate transformation (e.g., Welander 1963, section 4). The purpose here is to incorporate momentum diffusion into Long's model in order to derive the KdV–Burgers equation (2). Batchelor (1973, section 3.5) provides a rationale for the introduction of momentum diffusion in a steady flow that was used previously by Blumen (1989) to examine mountain waves.

We first note that the quantity in square brackets in (A1) is the Bernoulli function

$$B = \frac{1}{2}(\nabla\psi)^2 + gz. \quad \text{(A3)}$$

Batchelor points out that in one-dimensional steady flow the integrated energy equation with viscous dissipation reduces to

$$\frac{1}{2}u^2 + gz = \nu\frac{\partial u}{\partial x}, \quad \text{(A4)}$$

where ν is the kinematic eddy viscosity coefficient. It is noted further that

$$B = B(\psi) = \nu\frac{\partial u}{\partial x} \quad \text{(A5)}$$

could be applied to two-dimensional flow in a transition layer, that is, the frontal zone. The principal point that is made is that the flow may be regarded as locally one-dimensional within the region of rapid change; the flow variables are locally uniform on each side of the transition region such that there is no net change in the value of $B(\psi)$ despite the effects of viscosity within the transition region. In the present context, the eddy stress, say $\tau = \nu\partial u/\partial z$, would be omitted. The implication of such an assumption will be examined below. Application to the present model consists of the introduction of

$$-\nu\frac{\partial u}{\partial x} = \nu\frac{\partial^2\psi}{\partial x\partial z} \quad \text{(A6)}$$

into the square bracketed term in (A1). It is then possible to repeat Long's (1965) analysis and to derive the KdV–Burgers equation.

The modification to Long's (1965) analysis is relatively minor. His basic nondimensional equation (15) becomes

$$\frac{\partial^2\delta}{\partial z^2} + \gamma\frac{\partial^2\delta}{\partial x^2} + \frac{\beta}{2}\left[\alpha\left(\frac{\partial\delta}{\partial z}\right)^2 + \alpha\gamma\left(\frac{\partial\delta}{\partial z}\right)^2 - 2\frac{\partial\delta}{\partial z} + \epsilon\frac{\partial}{\partial x}\frac{\partial\delta}{\partial z}\right] + \sigma^2\delta = 0, \quad \text{(A7)}$$

where $\delta = z - \bar z$ is the streamline displacement, $\gamma = (h/\Delta)^2$ is the ratio of the fluid depth to frontal width, $\beta = bh$ where b is defined in (A2), $\alpha = ah^{-1}$, where a is the disturbance amplitude, $\epsilon = \nu(U\Delta)^{-1}$ is the nondimensional eddy viscosity coefficient, and

$$\sigma^2 = \frac{gbh^2}{U^2} = \left(\frac{N}{Uh^{-1}}\right)^2, \quad \text{(A8)}$$

[2] The compressible case has been considered by Scorer (1955) and Blumen (1988), but this feature is not important here.

where $N = gb$ is the Brunt–Väisälä frequency. The parameter σ is of order unity, and the other parameters are relatively small, such that the expansion

$$\delta = \delta_{00} + \alpha\delta_{10} + \beta\delta_{01} + \cdots$$

may be used to find solutions of (A7). Long shows that

$$\delta_{00} = f(x)\sin n\pi z, \tag{A9}$$

where $f(x)$ is to be determined.

Consider $\epsilon = 0$ for the moment. Long seeks solitary wave disturbances by balancing dispersion and nonlinearity. This balance is achieved in (A7) by a balance between the terms $\partial^2\delta/\partial x^2$ and $(\partial\delta/\partial z)^2$ in (A7). The requirement is that $\gamma = \alpha\beta$ in the expansion process. Solitary wave solutions are found at this order for n odd in (A9). Solutions for n even require that $\gamma = \alpha\beta^2$.

We now seek a balance between dispersion, nonlinearity, and momentum diffusion from (A7). The first approach is to assume that $\alpha = \epsilon$ and $\gamma = \alpha\beta = \epsilon\beta$. The three-way balance cannot be achieved at this order; it is necessary to require

$$\gamma = \alpha\beta^2 = \epsilon\beta^2. \tag{A10}$$

The development used by Long may now be carried out with minor modifications to show that

$$f'' + \sigma_{12}^2 f - \frac{n\pi f^2}{6} - \frac{f'}{2n\pi} = 0, \tag{A11}$$

where $\sigma_{12}^2 = -n\pi/9$ and n may be even or odd. Equation (A11) provides solitary wave solutions when the last term is omitted. Equation (A11) is a form of Fisher's equation (Sachdev 1987, section 4.2). Differentiation with respect to x, followed by a simple linear transformation of dependent and independent variables, cast (A11) into the form of the KdV–Burgers equation (2).

Other representations of frontal zone dynamics are possible. For example, Long (1971) considered a homogeneous fluid model but retained the earth's rotation. The counterpart of (A7), with $\epsilon = 0$, is provided by Long's equation (14). This model could, for example, represent a well-mixed frontal zone with an Ekman suction velocity w_0 at the lower boundary that flows vertically through the frontal zone. The parameter b in this case is represented by $b = (\ln w_0)_z$, and the horizontal streamline displacement δ is directly proportional to the alongfront velocity v. Further, the counterpart of (A8) is

$$\sigma^2 = \left(\frac{f_0}{w_0 h^{-1}}\right), \tag{A12}$$

where f_0 is the coriolis parameter. The procedure for establishing the existence of solitary wave solution is similar to that outlined above.

The procedure for the incorporation of momentum diffusion may also follow the aforementioned approach. Since the streamlines are essentially vertical, integration along a streamline provides, in analogy with (A5),

$$\beta(\psi) = \nu\frac{\partial w}{\partial z}. \tag{A13}$$

The term $v\,\partial w/\partial z = \nu\partial^2\psi/\partial x\partial z$ is introduced into the basic equation as in the development of (A7).

Again the omission of a stress, say $\tau = \nu\partial u/\partial z$, should be questioned. It is possible, in fact, to include all the viscous stresses in the foregoing analysis, but the procedure is laborious. Both Johnson (1972) and Mei (1966), for example, have considered the modification of solitary-wave evolution equations by means of frictional dissipation. It is only the Burgers type viscous term retained in (A5) or (A13) that provides the balance among dispersion, nonlinearity, and momentum diffusion. This result could probably be anticipated from (A4), which leads directly to Burgers equation in the absence of dispersion. However, the complete solution of the motion field in the frontal zone will involve all the viscous terms, including the term that provides the solitary wave. The complete solution will not be considered here. The present purpose is, however, only to establish that (2) represents a rational model of the frontal zone that may be matched to the inviscid region surrounding it.

APPENDIX B

Phase Plane Analysis

The phase plane analysis of (10) follows, in essence, that of Grad and Hu (1967). The transformation

$$w = \frac{\partial V}{\partial y} \tag{B1}$$

is introduced into (10) to obtain

$$\lambda\frac{\partial w}{\partial y} = \frac{1}{\lambda}\left[w + \tfrac{1}{2}(V+H)(V-H)\right]. \tag{B2}$$

The critical points of (B1) and (B2) are

$$\left.\begin{aligned}\text{upstream:}\quad & w = 0, \quad V = -H\\ \text{downstream:}\quad & w = 0, \quad V = H\end{aligned}\right\}. \tag{B3}$$

The local behavior at the upstream critical point may be established by letting $V = -(H - \delta)$, with $\delta \ll H$. The eigenvalues of (B1) and (B2) are provided by

$$\gamma = (2\lambda)^{-1}[1 \pm (1 - 4\lambda H)^{1/2}]. \tag{B4}$$

If

$$\lambda H \leqslant \tfrac{1}{4}, \tag{B5}$$

the upstream critical point is an *unstable nodal point* for increasing values of y; it is an *unstable spiral point* if

$$\lambda H > \tfrac{1}{4}. \tag{B5}$$

The local behavior downstream is determined by letting $V = H - \delta$, with $\delta \ll H$. The eigenvalues, in this case, are

$$\gamma = (2\lambda)^{-1}[1 \pm (1 + 4\lambda H)^{1/2}]. \quad \text{(B6)}$$

As demonstrated by Grad and Hu and by Johnson (1970), the downstream critical point is a *saddle point.* This analysis establishes that if $\lambda H \leqslant \frac{1}{4}$, the solution of (10), $V(y)$, increases monotonically with increasing y. The analytic solution for $\lambda = 0$ appears in I. If $\lambda H > \frac{1}{4}$, then a wave train appears upstream, that is, behind the front.

The trajectory that approaches the downstream critical point, $V = H$, is associated with $V > 0$, $w > 0$. Introduction of (B1) and (B4) and noting that $V = H - \delta$, yields

$$\frac{dV}{dy} = -\gamma\delta = -(2\lambda)^{-1}[1 - (1 + 4\lambda H)^{1/2}]\delta > 0. \quad \text{(B7)}$$

The initial values for the numerical integrations (V, dV/dy) are associated with $\delta = 10^{-4}$.

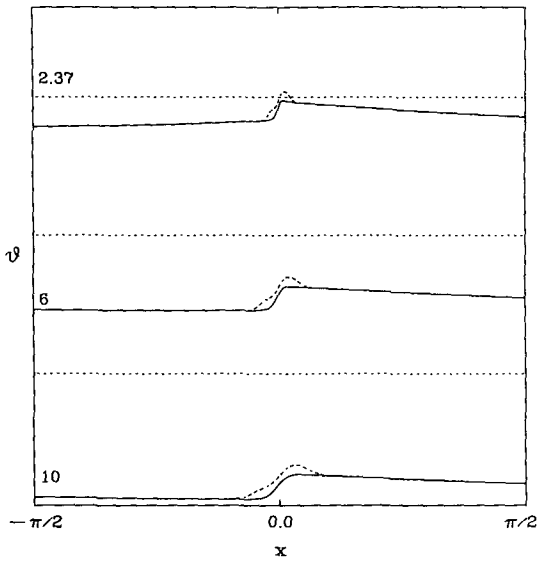

FIG. 9. Potential temperature $\theta \propto \Theta\tau$, defined by (B1), (solid) as a function of the horizontal coordinate x at ground level $z = -0.5$. The dashed curves show the incorrect distribution of θ that was displayed in I. The time τ appears along the left ordinate.

APPENDIX C

Corrigenda

The expression for V, the alongfront velocity, is provided by (10a,b) in I. The inviscid part V is a function of the spatial variable x, but the frontal zone contribution is only a function of the stretched variable $y = x/\epsilon$. Consequently, in the evaluation of Θ represented by (B16) in I, the frontal zone contribution should be evaluated by $(1 + \tau\partial V/\partial y)^{-1}\partial V/\partial y$ rather than by $(1 + \tau\partial V/\partial x)^{-1}\partial V/\partial x$. The correct expression for Θ, provided by (B18), is

$$\Theta = \left\{ V \operatorname{sech}^2 kz - \left[\cos(x + \delta + V_1\tau) + \frac{\frac{H(\tau)^2}{2} \operatorname{sech}^2\left[\frac{H(\tau)}{2\epsilon}(x + \delta)\right]}{1 + \tau\frac{H(\tau)^2}{2} \operatorname{sech}^2\left[\frac{H(\tau)}{2\epsilon}(x + \delta)\right]} \right] \times \left(\frac{a}{b} + \frac{b}{a}\right) \tanh kz \right\} \times \left[\left(1 + \left(\frac{a}{b}\right)^2 \tanh^2 kz\right)\left(1 + \left(\frac{b}{a}\right)^2 \tanh^2 kz\right)\right]^{-1/2}. \quad \text{(C1)}$$

The only change that occurs in (C1) is the omission of ϵ in the denominators of the $H(\tau)^2$ terms. The quantity δ in (C1) is a phase that is removed at $z = -0.5$ by a translation of the x coordinate.

The maximum error occurs at ground level, $z = -0.5$. The error decreases with increasing z, vanishing at $z = 0$. The solution at $z = -0.5$, corresponding to $\lambda = 0$, appears in Fig. 9. The solid curve is determined from (C1). The incorrect solution, displayed in Fig. 3 of I, is represented by the dashed curve. It is apparent that the error appearing in I is relatively small and does not affect any results presented in I.

Inadvertent misprints appear in II. The Table 2 entry associated with $z = -0.25$ appearing in column 3 should be 2.077 rather than 2.016.

The limits of the x integrations appearing in Eqs. (11), (13), (14), (16), (22), and (23) are $(-\pi, \pi)$, not $(-\Delta x/2, \Delta x/2)$. The evaluations appearing in II, and presented in Figs. 1 and 2, have been carried out with the correct limits $(-\pi, \pi)$, and the third column in Table 2 is also correct. Most of the contribution to each integral does, however, arise from the frontal zone of width Δx.

REFERENCES

Batchelor, G. K., 1973: *An Introduction to Fluid Dynamics.* Cambridge Press, 615 pp.

Blumen, W., 1988: Wave breaking in a compressible atmosphere. *Geophys. Astrophys. Fluid Dyn.*, **43**, 311–332.

——, 1989: Finite-amplitude mountain waves in a compressible atmosphere including the effects of dissipation. *Geophys. Astrophys. Fluid Dyn.*, **52**, 89–104.

——, 1990a: A semigeostrophic Eady-wave frontal model incorporating momentum diffusion: Part I. Model and solutions. *J. Atmos. Sci.*, **47**, 2890–2902.

——, 1990b: A semigeostrophic Eady-wave frontal model incorporating momentum diffusion: Part II. Kinetic energy and enstrophy dissipation. *J. Atmos. Sci.*, **47,** 2903–2908.

Christie, D. R., 1989: Long nonlinear waves in the lower atmosphere. *J. Atmos. Sci.*, **46,** 1462–1491.

Grad, H., and P. N. Hu, 1967: Unified shock profile in a plasma. *Phys. Fluids,* **10,** 2596–2602.

Johnson, R. S. 1970: A nonlinear equation incorporating damping and dispersion. *J. Fluid Mech.*, **42,** 49–60.

——, 1972: Shallow water waves on a viscous fluid—the undular bore. *Phys. Fluids,* **15,** 1693–1699.

Karpman, V. I. 1975: *Nonlinear Waves in Dispersive Media.* Pergamon, 186 pp.

Kennedy, P. J., and M. A. Shapiro, 1980: Further encounters with clear air turbulence in research aircraft. *J. Atmos. Sci.*, **37,** 986–993.

Keyser, D., and M. A. Shapiro, 1986: A review of the structure and dynamics of upper-level frontal zones. *Mon. Wea. Rev.*, **114,** 452–499.

Long, R. R., 1953: Some aspects of the flow of stratified fluids. I. A theoretical investigation. *Tellus,* **5,** 42–57.

——, 1965: On the Boussinesq approximation and its role in the theory of internal waves. *Tellus,* **17,** 46–52.

——, 1971: Finite amplitude disturbances in a rotating fluid. *Tellus,* **23,** 82–85.

Mei, C. C., 1966: Nonlinear gravity waves in a thin sheet of viscous fluid. *J. Math. Phys.*, **45,** 266–288.

Nakamura, N., and I. M. Held, 1989: Nonlinear equilibration of two-dimensional Eady waves. *J. Atmos. Sci.*, **46,** 3055–3064.

Sachdev, P. L., 1987: *Nonlinear Diffusive Waves.* Cambridge Press, 246 pp.

Scorer, R. S., 1955: Theory of non-horizontal adiabatic flow in the atmosphere. *Quart. J. Roy. Meteor. Soc.*, **81,** 551–561.

Uccellini, L. W., and S. E. Koch, 1987: The synoptic setting and possible energy sources for mesoscale wave disturbances. *Mon. Wea. Rev.*, **115,** 721–729.

Welander, P., 1963: Steady plane fronts in a rotating fluid. *Tellus,* **15,** 33–43.